Surface & Coatings Technology 206 (2011) 1963–1970

Contents lists available at SciVerse ScienceDirect

Surface & Coatings Technology

journal homepage: www.elsevier.com/locate/surfcoat

Multi-functional ECR plasma sputtering system for preparing amorphous carbon and Al–O–Si films

Xue Fan, Dongfeng Diao *, Kai Wang, Chao Wang

Key Laboratory of Education Ministry for Modern Design and Rotor-Bearing System, School of Mechanical Engineering, Xi'an Jiaotong University, Xi'an 710049, China

ARTICLE INFO

Available online 10 September 2011

Keywords:
DECR
MCECR
Double-target source
Shutter slider
Amorphous carbon film
Al–O–Si film

ABSTRACT

A design of cylindrical double-target source with shutter slider which can continuously change the target area ratio was applied to the divergent and mirror-confinement Electron Cyclotron Resonance (ECR) plasma sputtering system in the present study. The deposition process feasibility of several types of films (single-layer of pure and composite film as well as multi-layer film) can be realized by using this multi-functional system. The highly concerned amorphous carbon films were prepared with the Divergent ECR (DECR) and Mirror-Confinement ECR (MCECR) plasma sputtering systems. The tribological properties were compared, which both showed a normally friction coefficient around 0.15. Through adding substrate heating during film preparation, the tribological properties of DECR carbon films were improved with an obvious decreasing of friction coefficient to 0.05 and a much longer wear lifetime. The designed double-target source with shutter slider was used to prepare Al–O–Si films, by which the target area ratio of silicon to aluminum was changed from 0.5 to 2. A composite structure of Al–O–Si film with high transmittance up to 89% at 193 nm wavelength was obtained with the multi-functional ECR plasma sputtering system.

1. Introduction

Electron Cyclotron Resonance (ECR) plasma source is widely used in kinds of thin film processes, including the film deposition [1,2], etching [3], surface modification [4], doping [5], and epitaxy [6]. ECR plasma sputtering has the merits of low sputtering temperature, high plasma density, high degree of ionization and low working pressure, which provides a method for preparing thin solid films with low surface damage for industrial applications.

Divergent ECR (DECR) plasma sputtering deposition apparatus with solid material target was developed in 1984 [7], and oxidized metal films of Al_2O_3, Ta_2O_5, ZnO were prepared by using the DECR apparatus [8,9]. During the development of ECR application technique, Matsuoka and Ono discussed the effect of Mirror-confinement magnetic field application on ion energy of ECR plasma, which showed that ions with lower energy generated in the Mirror-Confinement ECR (MCECR) plasma comparing with the DECR plasma [10]. The MCECR plasma enhanced sputtering discharge for film deposition was investigated by Misina and coworkers [11], and $SrTiO_3$ (STO) and (Ba, Sr)TiO_3 (BST) films were prepared with the MCECR plasma sputtering for the dynamic random access memories [12,13]. In order to meet the requirement of semiconductor technology, ECR plasma sputtering with two plasma sources was investigated to deposit the SiO_2–Ta_2O_5 multilayered optical films [14]. In recent years, optical films with higher transmittance at 193 nm wavelength are important to support the laser optical parts within the system of micromachining and lithography [15]. Film materials like SiO_2, Al_2O_3 and so on showed high transmittance at wavelength of 193 nm, but multi-layers consisting of twenty or more layer pairs were necessary [16,17]. Therefore, single layer of Al–O–Si composite film combining the good performances of SiO_2 and Al_2O_3 with high transmittance is expected to deposit with simpler preparation method.

Hirono et al. investigated the effect of ion irradiation on the wear of DECR plasma sputtering carbon films by using the Atomic Force Microscope (AFM) scratch test with diamond tip radius of 80 nm, and the results showed that far superior hardness was obtained compared to that of RF sputtering films by removing weakly bonded carbon atoms using ion irradiation [18]. They deposited a new kind of super hard conductive nano-crystallite carbon film whose hardness (evaluated by the wear depth using AFM scratch test) is comparable to diamond hardness, while the conductivity is 19 orders of magnitude larger than that of diamond [19]. Diao and Hirono performed a joint study on the tribological properties of the carbon films prepared by DECR plasma sputtering, and the results showed that the friction coefficients were about 0.15 and the wear lifetimes were about hundreds or few thousands cycles, which were not good enough as a wear resistant layer [20]. Diao and Miyake also examined the tribological properties of carbon films prepared by MCECR plasma sputtering, and the best result obtained was the lowest friction coefficient of 0.11 and the longest wear lifetime of 3900 cycles [21]. The tribological properties of ECR carbon films still need to be improved to satisfy the requirement of industrial applications as a protective layer.

* Corresponding author. Tel./fax: +86 29 8266 9151.
E-mail address: dfdiao@mail.xjtu.edu.cn (D.F. Diao).

0257-8972/$ – see front matter © 2011 Elsevier B.V. All rights reserved.
doi:10.1016/j.surfcoat.2011.09.001

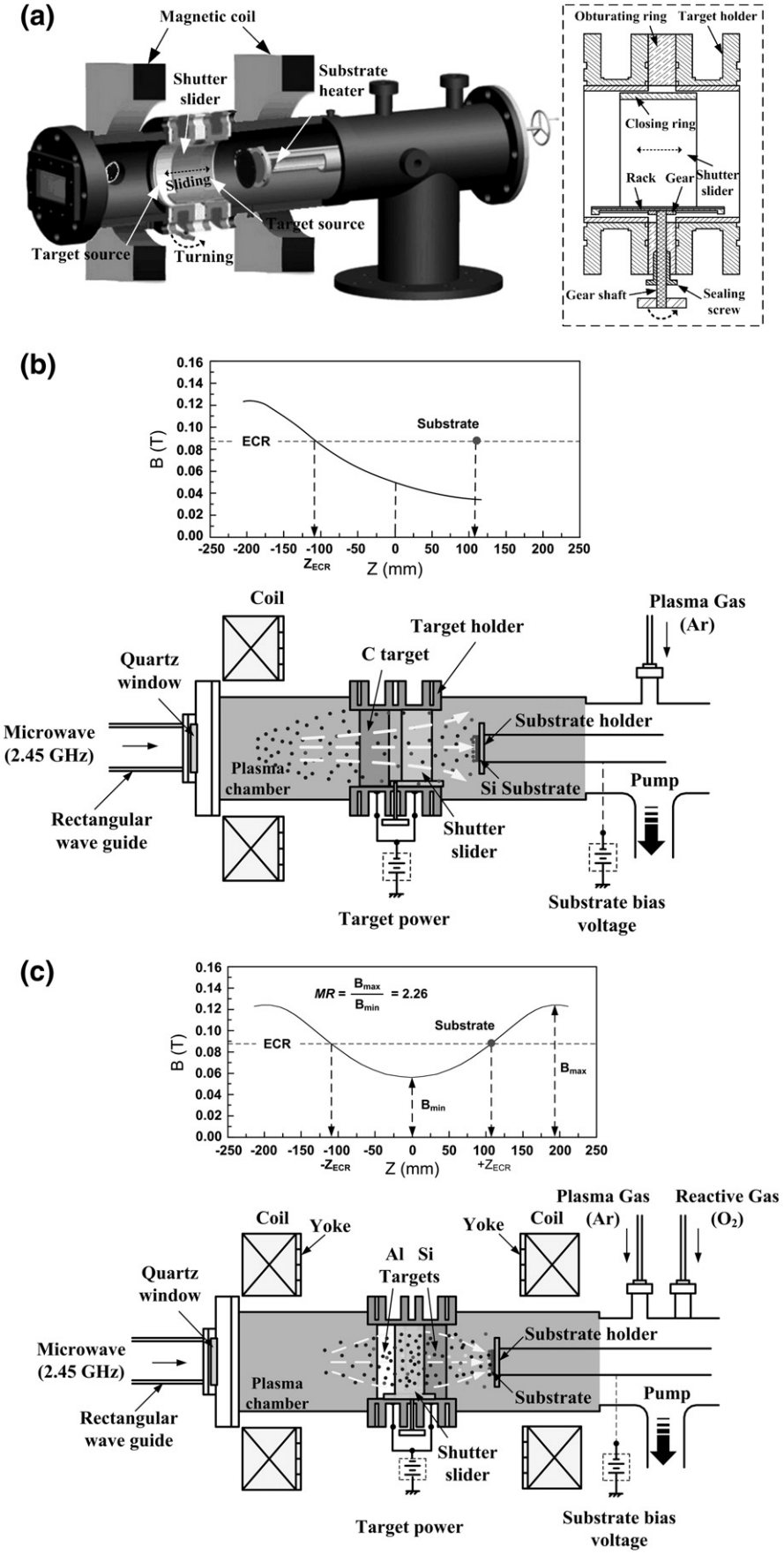

Fig. 1. Schematic illustrations of the multi-functional ECR plasma sputtering system, (a) Three- dimensional schematic of the ECR plasma sputtering apparatus including a double-target source with shutter slider (left), and the detail structure of shutter slider (right); (b) Schematic of DECR with magnetic flux density distribution; (c) Schematic of MCECR with magnetic flux density distribution.

Based on the above research background on ECR plasma sputtering technologies, in the present study, a cylindrical double-target source with shutter slider is applied to the ECR plasma sputtering system, and the multi-functional ECR system is used to prepare carbon films with better tribological properties and composite Al–O–Si films with high transmittance. For this purpose, plasma properties of DECR and MCECR are measured with Langmuir probe. Amorphous carbon and Al–O–Si films are deposited with the different functions of the apparatus. The nano structures and tribological properties of carbon films are characterized by Transmission Electron Microscope (TEM), X-ray Photoelectron Spectroscopy (XPS), and Pin-on-disk (POD) tribomoter. The structure, surface roughness and optical properties of Al–O–Si films are characterized by XPS, Atomic Force Microscope (AFM), and Deep Ultraviolet (DUV) spectral photometer.

2. Experiments

2.1. ECR configuration

Fig. 1 shows the three and two-dimensional schematic illustrations of the multi-functional ECR plasma sputtering system. In order to realize the preparation of composite single-layer films or multi-layer films with different targets in a limited space, a double-target source with shutter slider was designed as shown in Fig. 1(a). By adjusting the turning outside the chamber, the shutter slider can be moved along the surfaces of the cylindrical targets continuously, and the exposed areas of two targets are changed. Through using the shutter slider on the double target source, composite single-layer films can be deposited by exposing different area ratios of the two targets, or multi-layer films can be deposited by exposing different target each time. The shutter slider was made of steel and the surface was coated with a 0.2 mm thick alumina layer using the thermal sprayed method. In this study, 2.45 GHz microwave with the power of 200 W was introduced to the chamber through a rectangular waveguide and a fused quartz window. Magnetic coils were arranged around the chamber to achieve a microwave ECR condition (magnetic flux density, 875 G). DECR plasma was generated when the DC power was applied to the magnetic coil on left side (Fig. 1(b)), while MCECR plasma was generated when DC power was applied to both of the two coils (Fig. 1(c)). The magnetic coil current was set as 400 A, and the distance between the two magnetic coils was 390 mm, then the axial distributions of magnetic flux density B in DECR and MCECR plasma are shown in Fig. 1(b) and (c) respectively. The ECR zones lay at 110 mm away from the center of two targets, and substrate was located at the place of $Z=+110$ mm. As a result, the distance of substrate to the ECR zone (Z_{ECR}) of DECR was 220 mm, and that of substrate to the two ECR zones of MCECR ($-Z_{ECR}$, $+Z_{ECR}$) were 220 mm and 0 mm respectively. The substrate heater and thermocouple sensor fixed just behind the substrate holder can control the substrate temperature from room temperature to 700 °C.

The plasma properties with working pressures from 0.02 to 0.10 Pa for DECR and MCECR plasma were measured with Langmuir probe. The tungsten tip of 0.2 mm in diameter is located where the substrate is fixed during deposition. The Langmuir probe is floated in the plasma, and plasma density and potential are obtained from the current collected by the tip and the applied voltage. Results indicated that the plasma density of DECR was lower than that of MCECR, as shown in Fig. 2(a), the lower plasma density in DECR decreased collisions of ions with electrons and increased the sputtered ion energy. Besides, in the ECR plasma, when the ions transfer from strong magnetic field to the weaker field, they are accelerated (decelerated when the ions transfer from weaker to stronger field) by the force $F_z=-\mu_z \mathrm{grad}B_z$, where $\mu_z=mv^2/2B$, is the magnetic momentum of plasma volume unit, and $\mathrm{grad}B_z$ is the gradient of magnetic flux density B in the parallel Z direction to the magnetic field [22]. According to the magnetic flux distributions of DECR and MCECR shown in Fig. 1,

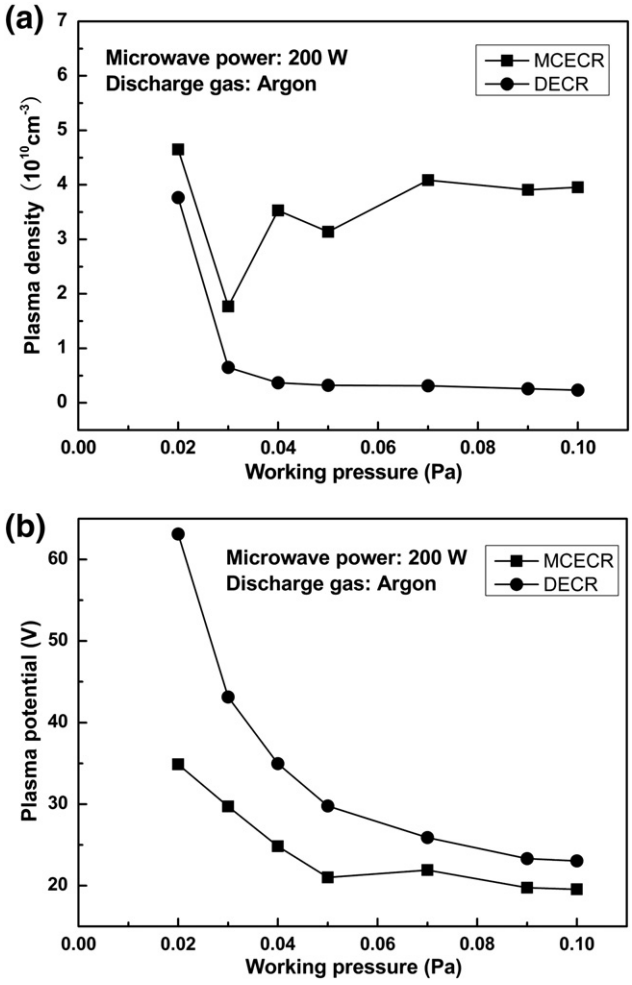

Fig. 2. Plasma properties of multi-functional ECR plasma sputtering system, (a) Plasma density; (b) Plasma potential.

ions are accelerated from the ECR zone to the substrate in DECR plasma, while in case of MCECR, ions will be decelerated before reaching the substrate, the ion energy in DECR plasma is higher. Fig. 2(b) shows the plasma potentials of DECR and MCECR plasma with different working pressures. The plasma potential formed in front of substrate is higher for DECR than MCECR at same working pressure. When the same substrate bias is applied, the energy of incident ion is higher in DECR plasma. As a result, the deposition rate will be decreased in the DECR plasma sputtering comparing with that of MCECR.

It is known that when a substrate is suspended into the plasma, a negative potential with respect to the plasma is built by the substrate, electrons are repelled and ions are accelerated to substrate by the voltage across the sheath, which directly influences the energy of incident ions. In the ECR plasma sputtering system, a modified Langmuir single probe, which has a large area simulated substrate near probe tip, was used to identify the electron irradiation by the coauthor. And the electron and ion irradiation scopes were clarified by comparing substrate bias voltage and the floating voltage which was obtained by the modified Langmuir probe [23]. During film deposition, substrate was insulated from the plasma chamber and connected to a DC power supply. Electric field was generated by the applied bias voltage which overlaid on the sheath potential. When the potential generated by positive bias voltage was higher than the sheath potential, substrate stayed at positive potential, ions were repelled and electrons reached the substrate, and when the potential was lower than the sheath potential, electrons were repelled and ions reached the substrate.

2.2. Deposition conditions

2.2.1. Carbon films prepared in DECR and MCECR plasma

Carbon films were deposited on p-type <100> oriented silicon substrates. Silicon substrates with the size 20 mm × 20 mm × 0.5 mm were first degreased in acetone, and then cleaned with absolute ethyl alcohol before put into the vacuum cavity. The background pressure of vacuum chamber was 3×10^{-4} Pa, and argon was inflated keeping the working pressure to be 0.04 Pa. The substrate surface was cleaned by Ar plasma for 3 min before target discharge voltage of −300 V (discharge current of 0.4 A) was applied. Carbon films were deposited in DECR and MCRCR plasma with substrate temperature starting at 21 °C, and increasing to about 60 °C after deposition. The DECR carbon films were deposited for 25 min, while the MCECR ones were deposited for 15 min. Another group of DECR carbon films was deposited with substrate heating at 400 °C for 25 min. The ECR carbon films were prepared with substrate bias voltages of +10 V, +20 V, +30 V, +50 V and +70 V.

2.2.2. Al–O–Si films prepared in MCECR plasma including double-target source with shutter slider

The fused-silica substrates (20 mm × 20 mm × 2 mm) were cleaned by ultrasonic wave and then put into the vacuum chamber. The chamber was pumped to a background pressure of 6.0×10^{-4} Pa with mechanical and molecular pumps. Then argon and oxygen gases controlled by mass flow meters were inflated to the working pressure of 0.04 Pa. Prior to deposition, substrate was pre-sputtered by argon plasma for 5 min with substrate bias voltage of −5 V, and then the targets were discharged with the voltage of −300 V and the current of 0.4 A. The Al–O–Si films were deposited only for 1 min because the deposition rate was high for the reactive sputtering deposition between Al, Si sputtered atoms and Oxygen by the effect of high activation of reactive gas and the ion irradiation. The films were prepared with substrate bias voltages of +20 V, +50 V and +80 V. Substrate temperature was room temperature of 21 °C. Groups of deposition conditions are shown in Table 1.

2.2.3. Characterizations

The bonding structures of deposited carbon films and composite Al–O–Si films were analyzed using X-ray photoelectron spectroscopy (XPS) with monochromatic Al Kα radiation (150 W, 15 kV, 1486.6 eV), and the film surfaces were cleaned by argon ions before the analysis. The nanostructures of carbon films were observed using Transmission Electron Microscopy (TEM) operated with the electron acceleration voltage of 300 kV (the two-point resolution is 0.17 nm). TEM specimens were prepared by mechanical polishing followed by argon ions beam milling to a thickness sufficient for TEM observation. The tribological properties of ECR carbon films were tested with pin-on-disk tribometer. Si_3N_4 ball with the radius of 3.17 mm was chosen as the counter pin, which was widely used in industrial applications as the ball bearing with low friction. The tribotests were performed with load of 2 N, disk rotational speed of 180 rpm and the friction radius of 1.4 mm.

The transmittance of Al–O–Si composite films at 193 nm wavelength was measured with Deep Ultraviolet (DUV) spectral photometer with the measurement wavelength from 180 to 1200 nm, which has high sensitivity in the ultraviolet band. Surface topographies of fused-silica and Al–O–Si films were measured by Atomic Force Microscope (AFM) with scan size of 1 μm × 1 μm, scan frequency of 0.75 Hz and the loaded force of 2–4 μN.

Table 1
Deposition conditions of Al–O–Si composite thin film, and the transmittance characterization at 193 nm wavelength.

No.	Deposition conditions			Characterization
	Exposure area ratio of Si to Al targets	Oxygen pressure (%)	Substrate bias voltage (V)	Transmittance at 193 nm wavelength (%)
1	2:1	7	+20	70
2	2:1	7	+50	73
3	2:1	7	+80	60
4	2:1	10	+20	48
5	2:1	10	+50	53
6	2:1	10	+80	24
7	1:1	7	+20	84
8	1:1	7	+80	66
9	1:1	10	+20	70
10	1:1	10	+50	80
11	1:1	10	+80	77
12	1:2	7	+20	80
13	**1:2**	**7**	**+50**	**89**
14	1:2	7	+80	63
15	1:2	10	+20	62
16	1:2	10	+50	62
17	1:2	10	+80	50

3. Results

3.1. Carbon films prepared by DECR and MCECR plasma sputtering

Typical nano structure of the deposited carbon films is presented in Fig. 3. The nano structures of the three kinds of ECR carbon films were amorphous, and there were ultra thin interface layers of about 2.5 nm between Si substrate and carbon film. The thicknesses of DECR and MCECR carbon films without substrate heating were 26 nm and 40 nm respectively. With substrate heating, the thickness of DECR carbon film was 122 nm. Considering about the deposition time, the deposition rates were about 1 nm/min and 2.7 nm/min for DECR and MCECR carbon film without substrate heating respectively, and it was about 5 nm/min for DECR carbon film with substrate heating.

Fig. 4 shows the XPS analysis results. C1s spectra of the ECR carbon films were obtained, then the trigonal (sp^2) and tetrahedral (sp^3) carbon hybridizations of amorphous carbon films were quantitatively analyzed by decomposing the C1s spectrum into Gaussian–Lorentzian distributions, as shown in Fig. 4(a). Except for the main carbon hybridizations at binding energy of 284.4 and 285.2 eV representing for the sp^2 and sp^3 bonds respectively, another two peaks of much smaller intensity at 286.6 and 288.8 eV have also been noticed which were attributed

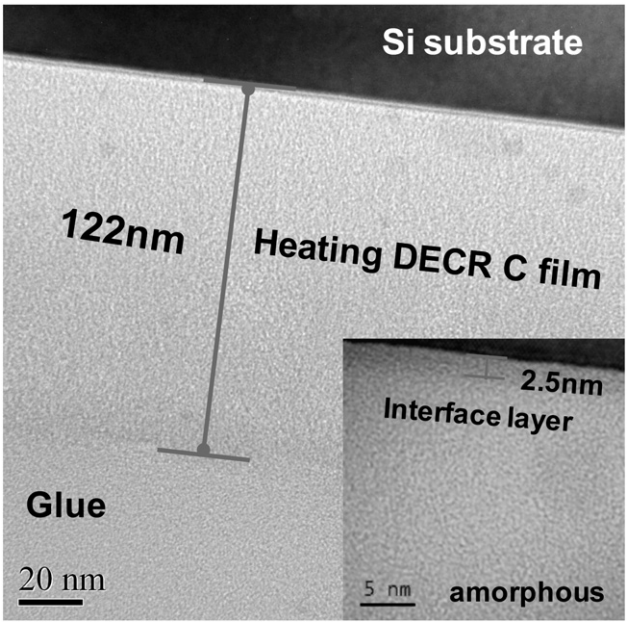

Fig. 3. Cross-sectional TEM pictures of a representative ECR carbon film (DECR carbon film with substrate heating at 400 °C).

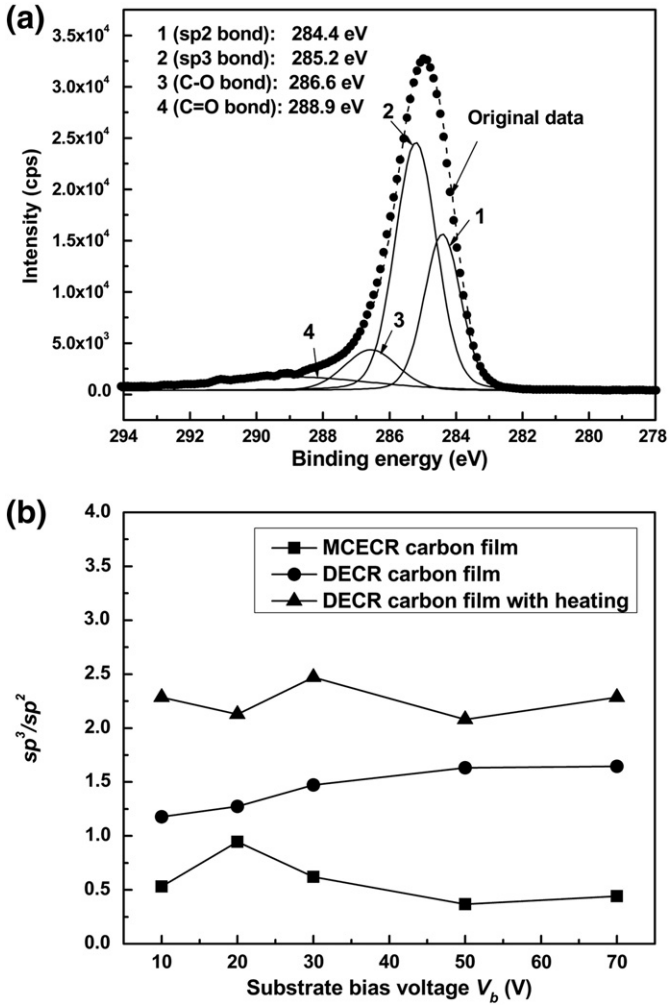

Fig. 4. The XPS analysis results of ECR carbon films with different substrate bias voltages, (a) The peak fitting result of C1s spectrum; (b) The content ratios of sp^3 to sp^2.

to some carbon atoms bonded with oxygen atoms on the film surface. The sp^3/sp^2 bonding ratio with different substrate bias voltages are summarized and shown in Fig. 4(b). The fraction of sp^3 bonds was higher than that of sp^2 for the DECR carbon films. According to the plasma measurement results, the energy of incident ions is higher during the DECR plasma sputtering, therefore, the formation of sp^3 bonds is easier for the DECR carbon films. The sp^3/sp^2 bonding ratio increased in the DECR carbon films with substrate heating comparing with the films without substrate heating. It has been studied that the thermal stability of amorphous carbon films is related to the sp^3 fraction, when the sp^3 fraction is higher in the film, the structure is more stable [24,25]. The conversion of sp^3 to sp^2 bonds did not happen in the DECR carbon films with substrate heating at 400 °C, which showed the thermal stability of ECR carbon films.

The typical friction curves of ECR carbon films are shown in Fig. 5. For the films without substrate heating, the friction coefficient tended to be stable after the running in stage, we took the mean value of stable stage friction coefficients as the friction coefficient of the sample, for example the friction coefficients of the MCECR and DECR samples without substrate heating in Fig. 5(a) and (b) were 0.154 and 0.175 respectively. The friction coefficient had two stable stages for the DECR carbon film with substrate heating, as shown in Fig. 5(c), in which the sample showed high friction coefficient of 0.206 and low friction coefficient of 0.062. All the DECR films prepared with substrate heating showed the obvious friction coefficient decreasing stage, while the films without substrate heating did not have such

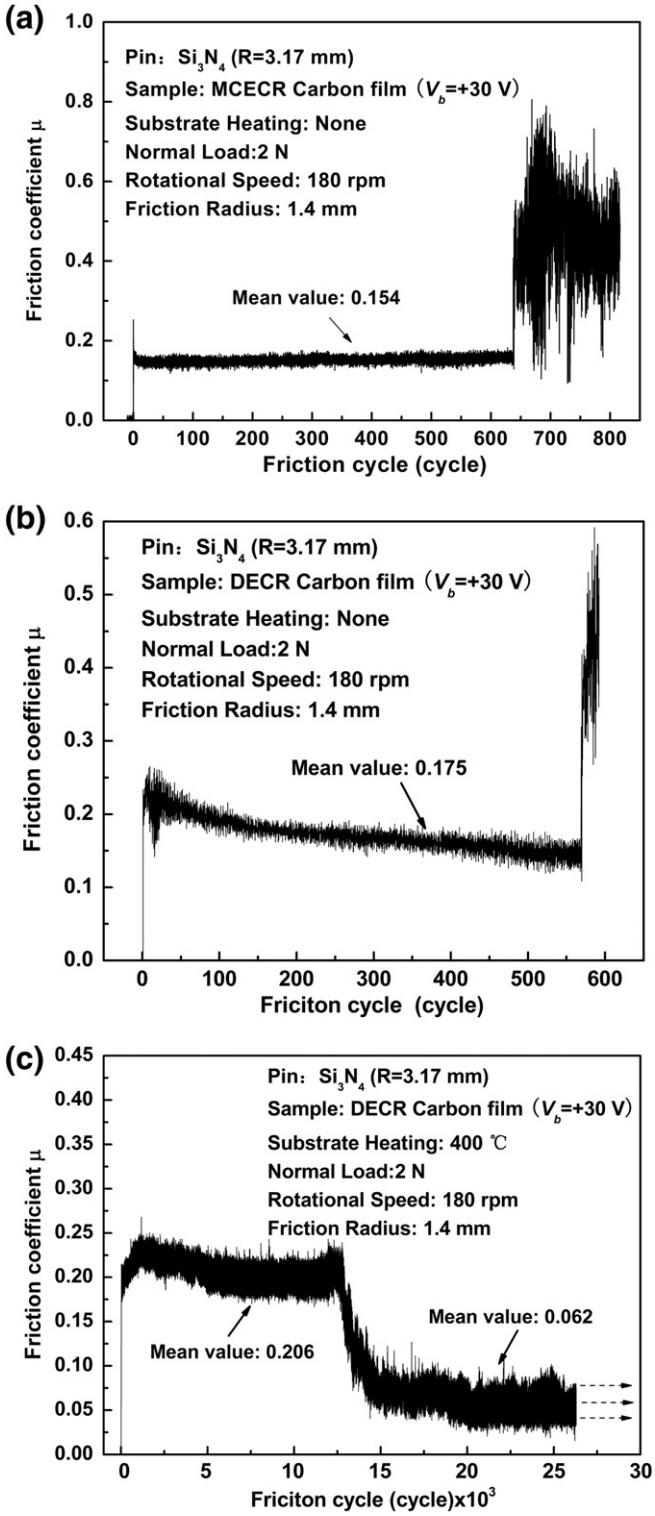

Fig. 5. Typical friction curves of the ECR carbon films, (a) MCECR carbon film without heating; (b) DECR carbon film without heating; (c) DECR carbon film with substrate heating.

character. Wear lifetime was obtained from the friction cycle before film worn out (for example, they were 639 and 592 cycles for the films in Fig. 5(a) and (b) respectively). The wear lifetime of DECR carbon film with substrate heating was so long that the failure of the film cannot be shown even at the end of the curve for 27,500 cycles, as shown in Fig. 5(c). The detailed explanations about the mechanisms of the long wear lifetime will be given in the discussion session.

The mean friction coefficients of the carbon films are summarized in Fig. 6(a). The friction coefficients of the MCECR and DECR carbon films without substrate heating were around the value of 0.15, which is typical for amorphous carbon films. While obvious friction coefficient decreasing during tribotests happened for the DECR carbon films with substrate heating, the high stable friction coefficients were also about 0.15, and the lower ones were near the value of 0.05. The mean wear lifetimes of the three kinds of carbon films are shown in Fig. 6(b). The wear lifetimes of the MCECR and DECR films without substrate heating were relative low with few to tens of hundreds of cycles. However, the DECR carbon films with substrate heating cannot be worn out at 15,000 cycles. With the multi-functional ECR plasma sputtering system introduced in this paper, amorphous carbon films with good tribological properties of low friction coefficient to 0.05 and long wear lifetime were prepared.

3.2. Al–O–Si composite films prepared by the double-target source with shutter slider

Al–O–Si composite films were prepared by using the double-target source with shutter slider in the MCECR plasma sputtering system. The thickness of Al–O–Si film was about 60 nm with the deposition rate of 60 nm/min. The transmittance of the films at 193 nm wavelength was measured with DUV spectral photometer, and the results are summarized in Table 1. Film deposition conditions seriously affected the transmittance, which varied between 24% and 89%. When the area ratio of silicon to aluminum targets was 1:2, substrate bias voltage was +50 V and oxygen pressure was 7%, the highest transmittance of Al–O–Si films at 193 nm was obtained to be 89%.

To study the composite structure of Al–O–Si film with high transmittance of 89%, XPS spectra of Al2p, O1s, and Si2p of the sample were measured as shown in Fig. 7. The peak fitting result of Al2p spectrum (Fig. 7(a)) showed only one peak located at 74.8 eV, which was much different with the 73.1 eV Al2p peak in aluminum, and slightly higher than the 74.4 eV Al2p peak in Al_2O_3 [26]. The single peak in Al2p spectrum indicated that Al element existed in the film with one-phase composite. The binding energy of Al2p in the Al–O–Si film was different from those in pure aluminum and alumina and other related aluminum compounds, which meant that the composite structure of Al in Al–O–Si film was neither aluminum nor alumina. The peak fitting results of O1s (Fig. 7(b)) and Si2p (Fig. 7(c)) also showed that only one binding peak existed with the peak position at 531.5 eV and 103.0 eV respectively. The O1s binding energy is between those of the Al_2O_3 (531.0 eV) and SiO_2 (533.0 eV), and the Si2p binding energy in the Al–O–Si film is between those of the pure silicon (99.5 eV) and SiO_2 (103.5 eV). The binding peak of pure aluminum, pure silicon, Al_2O_3 and SiO_2 cannot be found in the XPS spectra of Al2p, O1s and Si2p, and each binding energy of the three elements in the film was appeared with only one fitting peak. Therefore, a one-phase

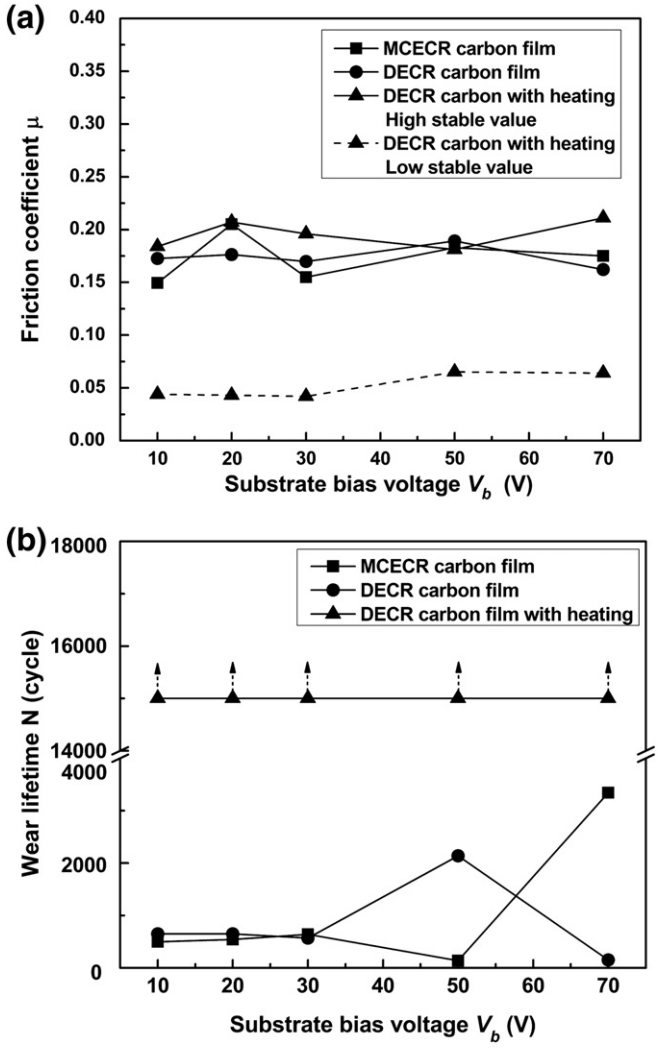

Fig. 6. Tribological properties of the ECR carbon films with different substrate bias voltages, (a) Friction coefficients; (b) Wear lifetimes.

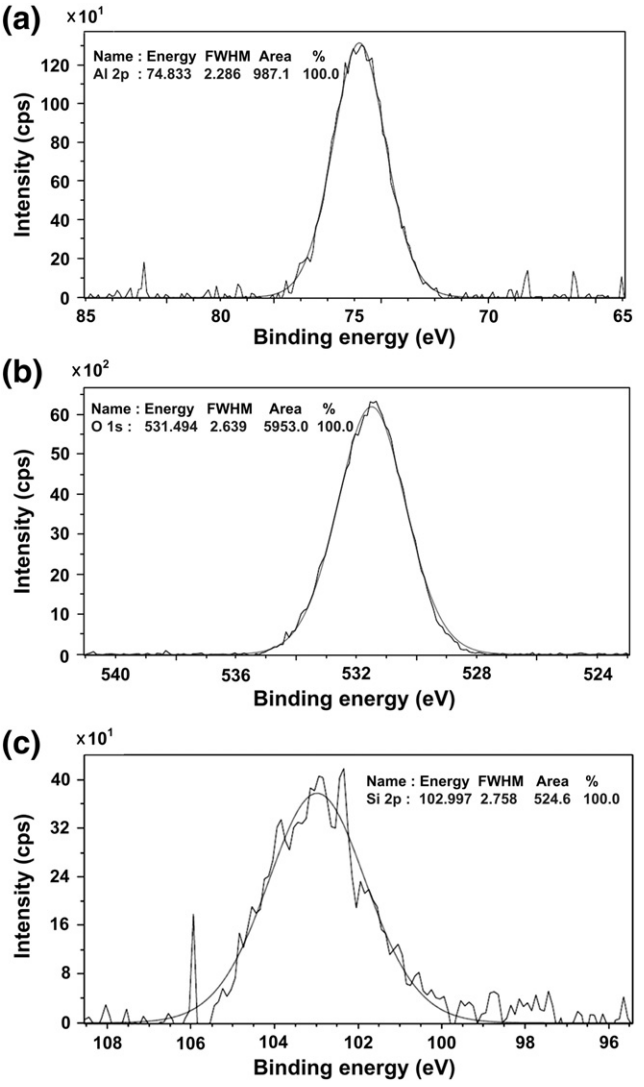

Fig. 7. Al2p (a), O1s (b), and Si2p (c) XPS spectra of MCECR Al–O–Si film.

composite structure of Al–O–Si film was deposited by using the double-target source with shutter slider in the MCECR plasma sputtering system.

Surface topographies of fused-silica substrate and Al–O–Si films deposited with different preparation parameters are shown in Fig. 8. There were sharp peaks and obvious grooves left at the polished fused-silica substrate surface (Fig. 8(a)). After deposited a single layer of Al–O–Si films, the surface was quite smooth (Fig. 8(b)) with the maximum surface roughness of 1.26 nm when the area ratio of Si to Al targets was 1:2, substrate bias voltage was +50 V and oxygen pressure was 7%, and there were only slight fluctuations on the film surface. In Fig. 8(c), many domes appeared on the film surface when the sample was deposited with the area ratio of 1:1, substrate bias voltage of +50 V and oxygen pressure of 10%, and the maximum surface roughness was 1.51 nm. The grooves disappeared and the sharp peaks still existed when the area ratio of Si to Al targets was 2:1, substrate bias voltage was +50 V, and oxygen pressure was 7% (Fig. 8(d)), the maximum surface roughness was 2.45 nm. All the grooves, peaks, fluctuations and domes distributed randomly on the film surface. According to the result of the transmittance at 193 nm wavelength (Table 1), the sample in Fig. 8(b) had the highest transmittance and the lowest surface roughness, and the transmittance decreased with the increasing of surface roughness for the films in Fig. 8(c) and (d), which indicated that the optical property of Al–O–Si films was affected by the surface topography, especially the sharpness degree of the maximum values of the surface roughness.

4. Discussion

In the present study, a cylindrical double-target source with shutter slider was applied to the DECR and MCECR plasma sputtering system, and the multi-functional ECR system was used for preparing carbon film with better tribological properties and composite Al–O–Si film with high transmittance. Usually, a target with constant elements content ratio was used to obtain only one kind of thin film with fixed elements content ratio, therefore lots of targets were needed in order to study the effect of elements content ratio on the required properties of composite films. On the other hand, to obtain multi-layers films with the ECR plasma sputtering method, two or more plasma source sputtering chambers that contained different targets were used before. Therefore, the multi-functional ECR plasma sputtering system was introduced to solve equipment problems in this paper.

During the ECR plasma sputtering, the neutral sputtered atoms are easily contaminated at the quartz window, which will affect the introduction of microwave into the chamber. In a developed ECR plasma source, microwaves were divided into two directions with equal power and then introduced to a microwave composer through quartz windows over the same distance, and the quartz windows were set blind from the ECR plasma. Results indicated that the design could effectively prevent film deposition on quartz windows and keep microwave source with high stability [27]. Narrow corner waveguide with a double bend to set the quartz window blind was also investigated that can effectively prevent the pollution to the quartz window [11]. In the present study, quartz window was placed directly perpendicular to the magnetic flux direction to seal the vacuum. Microwave reflected power was monitored during the film deposition, and the quartz window was observed after deposition. It showed that there was only tiny pollution at the surface when preparing the carbon and Al–O–Si films, which did not affect the microwave reflected power during deposition.

Typical amorphous carbon films were prepared with MCECR and DECR plasma sputtering without substrate heating and DECR with substrate heating at 400 °C. The tribological properties were compared that the DECR carbon films with substrate heating exhibited improved tribological properties with low friction coefficient of 0.05 and long wear lifetimes. The thicknesses of samples we used here were different, and it is known that usually the thicker the film, the longer the wear lifetime for the films with same structure. Although the film thickness of DECR carbon film with substrate heating was 3–5 times thicker than the films without substrate heating, the

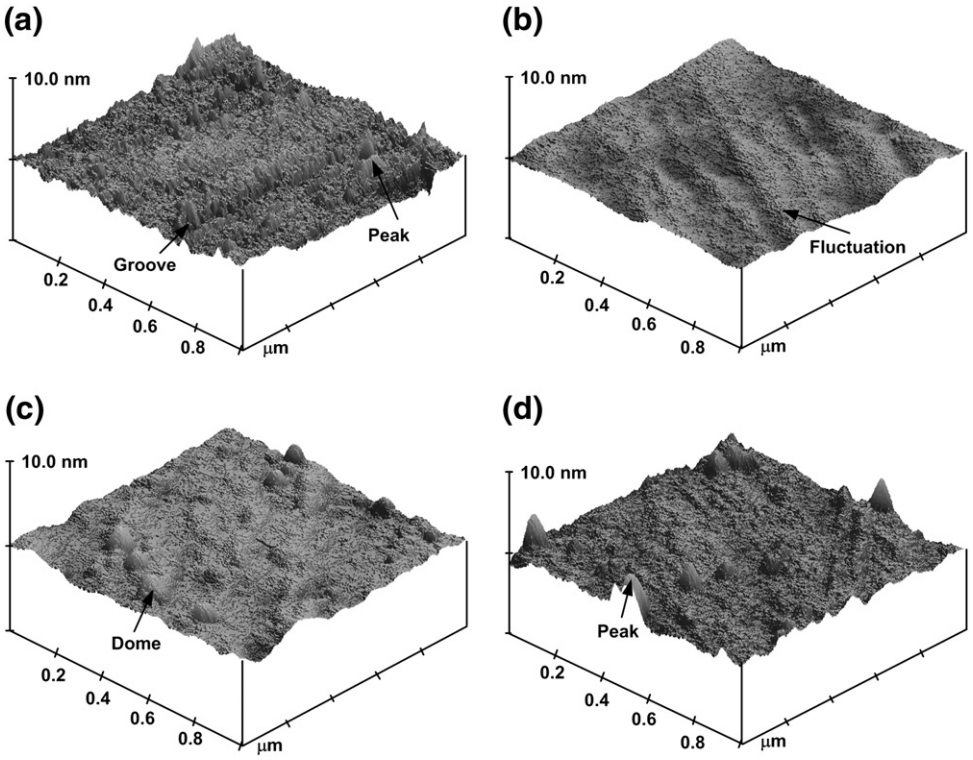

Fig. 8. Surface topographies of fused-silica and Al–O–Si films measured by AFM with scan size of 1 μm × 1 μm, (a) Fused-silica substrate; (b) Al–O–Si film: +50 V, 7%, 1:2; (c) Al–O–Si film: +50 V, 10%, 1:1; (d) Al–O–Si film: +50 V, 7%, 2:1.

wear lifetimes were more than 30 times longer. We have studied that the transfer layers formed during sliding wear and effectively decreased the friction coefficients and maximum contact stresses, which contributed to the long wear lifetime of DECR carbon films with substrate heating. Therefore, it is suggested that the MCECR and DECR amorphous carbon films without substrate heating cannot generate effective transfer layer during the sliding contact, which inhibited the appearance of friction coefficient decreasing and long wear lifetime.

During the deposition of Al–O–Si films, the percentage of oxygen has been examined and controlled in order to avoid the formation of alumina coating on the aluminum target surface, which would hinder the sputtering process. The targets were pre-sputtered for 10 min before film deposition, which not only cleaned the targets and shutter slider but also cleaned the environment of MCECR plasma in the vacuum chamber. Through applying the double-target source with a shutter slider to the ECR plasma sputtering system, single layer Al–O–Si composite films with high transmittance were successfully prepared, and the double-target source with shutter slider is going to be used for the preparation of multi-layer thin solid films in the future.

5. Conclusions

In this paper, multi-functional ECR plasma sputtering system including a cylindrical double-target source with shutter slider was introduced. Composite single-layer films or multi-layer films can be prepared with different exposing target areas through moving the shutter slider. By using the system, amorphous carbon films and composite Al–O–Si films were prepared.

The ECR carbon films showed amorphous structures. The friction coefficients of MCECR and DECR carbon films without substrate heating were near the value of 0.15. The DECR carbon films with substrate heating exhibited improved tribological properties with an obvious decreasing of friction coefficient to 0.05 and a much longer wear lifetime, which make the ECR carbon films can be more widely used in the field of tribological application.

One-phase composite Al–O–Si films were prepared by using the developed double-target source with shutter slider, and the film showed a high transmittance of 89% at 193 nm wavelength when the preparation conditions were area ratio of silicon to aluminum targets of 1:2, substrate bias voltage of +50 V and oxygen pressure of 7%. The optical property of Al–O–Si films at 193 nm was affected by the surface topography, and because of the low surface damage of MCECR plasma sputtering, Al–O–Si film with optimal optical property was obtained.

Acknowledgment

The authors would like to thank the National Nature Science Foundation of China with Grant Numbers of 90923027 and 51050110137, as well as the National High-Tech Research & Development Plan with Grant Number 2007AA04Z307 for their support.

References

[1] H. Akazawa, Thin Solid Films 518 (2009) 22.
[2] D. Xie, H.J. Liu, X.R. Deng, Y.X. Leng, N. Huang, Surf. Coat. Technol. 204 (2010) 3029.
[3] H.Y. Zhou, L. Wang, X.D. Zhu, B. Ke, F. Ding, X.H. Wen, Y.N. Yang, Rev. Sci. Instrum. 81 (2010) 033501.
[4] W. Tseng, C. Tseng, P. Chuang, A. Lo, C. Kuo, J. Phys. Chem. C 112 (2008) 18431.
[5] H. Akazawa, J. Vac. Sci. Technol. A 28 (2010) 314.
[6] Z. Yang, J.H. Lim, S. Chu, Z. Zou, J.L. Liu, Appl. Surf. Sci. 255 (2008) 3375.
[7] T. Ono, C. Takahashi, S. Matsuo, Jpn. J. Appl. Phys. 23 (1984) L534.
[8] C. Takahashi, M. Kiuchi, T. Ono, S. Matsuo, J. Vac Sci Technol. A6 (1988) 2348.
[9] M. Matsuoka, K. Ono, Appl. Phys. Lett. 53 (1988) 1393.
[10] M. Matsuoka, K. Ono, J. Vac. Sci. Technol. A6 (1988) 25.
[11] M. Misina, Y. Setruhara, S. Miyake, J. Vac. Sci. Technol. A15 (1997) 1922.
[12] S. Baba, K. Numatab, H. Saitob, M. Kumagai, T. Ueno, B. Kyoh, S. Miyake, Thin Solid Films 390 (2001) 70.
[13] S. Miyake, S. Baba, A. Niino, K. Numata, Surf. Coat. Technol. 169–170 (2003) 27.
[14] Y. Jin, M. Shimada, T. Ono, J. Vac. Sci. Technol. A 22 (2004) 2431.
[15] F.D. Lai, J.M. Hua, C.Y. Huang, F.H. Ko, L.A. Wang, C.H. Lin, C.M. Chang, S. Lee, G.W. Chern, Thin Solid Films 496 (2006) 247.
[16] H. Blaschke, M. Jupe, D. Ristau, Laser-Induced Damage in Optical Materials: 2002 and 7th International Workshop on Laser Beam and Optics Characterization, 4932, 2002, p. 467.
[17] H. Blaschke, M. Lappschies, D. Ristau, SPIE, Boulder, CO, USA, 2007 (67200 T).
[18] S. Hirono, S. Umemura, Y. Andoh, T. Hayashi, R. Kaneko, IEEE Trans. Magn. 34 (1998) 1729.
[19] S. Hirono, S. Umemura, M. Tomita, R. Kaneko, Appl. Phys. Lett. 80 (2002) 425.
[20] D.F. Diao, F. Iwata, S. Hirono, S. Umemura, Y.B. Xie, 3rd International Conference on Surface Engineering, Chengdu, China, 2002, p. 77.
[21] D.F. Diao, C.L. Cai, S. Miyake, T. Matsumoto, in: S. Miyake (Ed.), Novel Materials Processing by Advanced Electromagnetic Energy Sources, Elsevier Publisher, Japan, 2005, p. 87.
[22] J. Musil, Vacuum 47 (1996) 145.
[23] C. Wang, D.F. Diao, Surf. Coat. Technol. (2011), doi:10.1016/j.surfcoat.2011.08.009.
[24] R. Kalish, Y. Lifshitz, K. Nugent, S. Prawer, Appl. Phys. Lett. 74 (1999) 2936.
[25] A.C. Ferrari, B. Kleinsorge, N.A. Morrison, A. Hart, V. Stolojan, J. Robertson, J. Appl. Phys. 85 (1999) 7191.
[26] N. Koshizaki, H. Umehara, T. Oyama, Thin Solid Films 325 (1998) 130.
[27] T. Ono, H. Nishimura, M. Shimada, S. Matsuo, J. Vac. Sci. Technol. A 12 (1994) 1281.